Neurobiology of Disease

Oral Treatment with Cu^{II}(atsm) Increases Mutant SOD1 *In Vivo* but Protects Motor Neurons and Improves the Phenotype of a Transgenic Mouse Model of Amyotrophic Lateral Sclerosis

Blaine R. Roberts,[1]* Nastasia K. H. Lim,[2]* Erin J. McAllum,[2]* Paul S. Donnelly,[3,4] Dominic J. Hare,[1,6] Philip A. Doble,[6] Bradley J. Turner,[1] Katherine A. Price,[2] Sin Chun Lim,[3,4] Brett M. Paterson,[3,4] James L. Hickey,[3,4] Timothy W. Rhoads,[7,8] Jared R. Williams,[7,8] Katja M. Kanninen,[2] Lin W. Hung,[1,4] Jeffrey R. Liddell,[2] Alexandra Grubman,[2] Jean-Francois Monty,[10] Roxana M. Llanos,[10] David R. Kramer,[11] Julian F. B. Mercer,[10] Ashley I. Bush,[1] Colin L. Masters,[1] James A. Duce,[1,12] Qiao-Xin Li,[1] Joseph S. Beckman,[7,8,9] Kevin J. Barnham,[1,4,5] Anthony R. White,[1,2] and Peter J. Crouch[1,2]

[1]Florey Institute of Neuroscience and Mental Health, [2]Department of Pathology, [3]School of Chemistry, [4]Bio21 Institute of Biotechnology and Molecular Biology, and [5]Department of Pharmacology, The University of Melbourne, Parkville, 3010 Victoria, Australia, [6]Elemental Bio-imaging Facility, and Department of Chemistry and Forensic Science, University of Technology Sydney, 2007 Broadway, New South Wales, Australia, [7]Department of Biochemistry and Biophysics, [8]Linus Pauling Institute, and [9]Environmental Health Sciences Centre, Oregon State University, Corvallis, Oregon 97331, [10]Centre for Cellular and Molecular Biology, School of Life and Environmental Sciences, Deakin University, Burwood, 3125 Victoria, Australia, [11]ANU Medical School, ANU College of Medicine, Biology and the Environment, The Australian National University, 0200 Canberra, Australian Capital Territory, Australia, and [12]School of Molecular and Cellular Biology, University of Leeds, Leeds LS2 9JT, United Kingdom

Mutations in the metallo-protein Cu/Zn-superoxide dismutase (SOD1) cause amyotrophic lateral sclerosis (ALS) in humans and an expression level-dependent phenotype in transgenic rodents. We show that oral treatment with the therapeutic agent diacetyl-bis(4-methylthiosemicarbazonato)copper^{II} [Cu^{II}(atsm)] increased the concentration of mutant SOD1 (SOD1G37R) in ALS model mice, but paradoxically improved locomotor function and survival of the mice. To determine why the mice with increased levels of mutant SOD1 had an improved phenotype, we analyzed tissues by mass spectrometry. These analyses revealed most SOD1 in the spinal cord tissue of the SOD1G37R mice was Cu deficient. Treating with Cu^{II}(atsm) decreased the pool of Cu-deficient SOD1 and increased the pool of fully metallated (holo) SOD1. Tracking isotopically enriched $^{65}Cu^{II}$(atsm) confirmed the increase in holo-SOD1 involved transfer of Cu from Cu^{II}(atsm) to SOD1, suggesting the improved locomotor function and survival of the Cu^{II}(atsm)-treated SOD1G37R mice involved, at least in part, the ability of the compound to improve the Cu content of the mutant SOD1. This was supported by improved survival of SOD1G37R mice that expressed the human gene for the Cu uptake protein CTR1. Improving the metal content of mutant SOD1 *in vivo* with Cu^{II}(atsm) did not decrease levels of misfolded SOD1. These outcomes indicate the metal content of SOD1 may be a greater determinant of the toxicity of the protein in mutant SOD1-associated forms of ALS than the mutations themselves. Improving the metal content of SOD1 therefore represents a valid therapeutic strategy for treating ALS caused by SOD1.

Introduction

Amyotrophic lateral sclerosis (ALS) is a fatal adult-onset disease in which motor neurons in the spinal cord and brain progressively deteriorate and die. Initial clinical symptoms of ALS are relatively mild, but inevitably progress to paralysis and premature death as the extent of motor neuron failure increases. Riluzole (trade name Rilutek) is the only approved treatment for ALS, but its therapeutic effects are minimal. Treatment with riluzole provides an approximate 3 month increase in patient survival and has no effect on the deterioration of muscle strength (Bensimon

Received Sept. 30, 2013; revised April 30, 2014; accepted May 2, 2014.

Author contributions: B.R.R. and P.J.C. designed research; B.R.R., N.K.H.L., E.J.M., D.J.H., B.J.T., K.A.P., S.C.L., B.M.P., J.L.H., T.W.R., J.R.W., K.M.K., L.W.H., J.R.L., A.G., J.S.B., and P.J.C. performed research; P.A.D., J.-F.M., R.M.L., D.R.K., J.F.B.M., A.I.B., C.L.M., J.A.D., J.S.B., and P.J.C. contributed unpublished reagents/analytic tools; B.R.R., N.K.H.L., E.J.M., P.S.D., D.J.H., P.A.D., J.R.W., Q.-X.L., J.S.B., K.J.B., A.R.W., and P.J.C. analyzed data; B.R.R., N.K.H.L., E.J.M., P.S.D., and P.J.C. wrote the paper.

This work was supported by funds from the Australian National Health and Medical Research Council (Project Grants 1005651 and 1061550); the Motor Neuron Disease Research Institute of Australia; the Victorian Government Operational Infrastructure Support Program; Bethlehem Griffiths Research Foundation; the CASS Foundation; the Australian Research Council; the National Academy of Finland; the Sigrid Juselius Foundation; and The University of Melbourne.

*B.R.R., N.K.H.L., and E.J.M. contributed equally to this work.

A.I.B. is a paid consultant for Collaborative Medicinal Development LLC. Collaborative Medicinal Development LLC has licensed intellectual property on this subject from The University of Melbourne, where the inventors are P.S.D., K.J.B., and A.R.W. Some of the samples used for histology were prepared by the Biomedical Sciences Histology Facility, The University of Melbourne.

Correspondence should be addressed to Dr. Peter J. Crouch, Department of Pathology, The University of Melbourne, 3010 Parkville, Victoria, Australia. E-mail: pjcrouch@unimelb.edu.au.

K.M. Kanninen's present address: AI Virtanen Institute for Molecular Sciences, University of Eastern Finland, Kuopio 70211, Finland.

K.A. Price's present address: Department of Neuroscience, Icahn School of Medicine at Mount Sinai Hess Centre for Science and Medicine, 1470 Madison Avenue, New York, NY 10029.

DOI:10.1523/JNEUROSCI.4196-13.2014

 0270-6474/14/348021-11$15.00/0

et al., 1994; Lacomblez et al., 1996; Miller et al., 1996). The development of new treatment strategies for ALS is needed.

Approximately 90% of ALS cases are sporadic, and 10% are familial. Several genes are associated with the development of ALS, including *TARDBP* (Sreedharan et al., 2008) and *C9ORF72* (DeJesus-Hernandez et al., 2011; Renton et al., 2011), but the gene for the ubiquitous antioxidant enzyme Cu/Zn-superoxide dismutase (SOD1) is the most widely studied to date and has provided the basis for the development of the most robust animal models of ALS. Over 100 different SOD1 mutations account for ~20% of familial ALS cases (Rosen et al., 1993), and SOD1 mutations are also present in sporadic forms of the disease (Andersen et al., 2003). Nonmutated, wild-type SOD1 is aberrantly metabolized in sporadic cases of ALS (Bosco et al., 2010), and overexpression of wild-type SOD1 causes an ALS-like phenotype in mice that is comparable to the phenotype of ALS model mice caused by the expression of mutant SOD1 (Graffmo et al., 2013). Thus, the pathogenic role of SOD1 in ALS appears to extend beyond familial cases that involve SOD1 mutations.

Although oxidative damage is conspicuous in disease-affected tissues (Niebrój-Dobosz et al., 2004), SOD1 mutations do not cause ALS by a loss of antioxidant function (Bruijn et al., 1998). Motor neuron death in SOD1-associated forms of ALS therefore represents the consequences of a toxic gain of function in the mutant protein. Underscoring this, transgenic mice overexpressing mutant SOD1 develop an ALS-like phenotype that is proportional to the expression level of the mutant SOD1. Higher levels of mutant SOD1 cause earlier disease onset, more severe disease symptoms, and more rapid disease progression (Gurney et al., 1994; Wong et al., 1995; Henriques et al., 2010). However, despite the clear link between motor neuron death and disease symptoms in SOD1-associated forms of ALS, the fundamental basis of SOD1 toxicity in ALS is not fully understood. To address this, the present study examined spinal cord tissue collected from ALS model mice (SOD1G37R; Wong et al., 1995) that had been treated with the therapeutic agent diacetyl-bis(4-methylthiosemicarbazonato)copper^{II} [Cu^{II}(atsm)]. Given that the ALS-like phenotype of these mice is driven by expression of the mutant SOD1, the aim of the study was to investigate the relationship between therapeutic activity of Cu^{II}(atsm) and its effects on SOD1.

Materials and Methods

SOD1G37R mice. SOD1G37R mice (Wong et al., 1995) were used in this study. The effects of Cu^{II}(atsm) have been investigated previously in a G93A mouse model of ALS (Soon et al., 2011). SOD1G37R mice purchased from The Jackson Laboratory, and a colony was maintained by breeding SOD1G37R-positive mice with nontransgenic C57BL/6 mice. Mice were housed in standard boxes (two to five mice per box) with access to food and water *ad libitum*. Bedding for the boxes contained only saw dust and shredded paper, with no other environmental enrichment. Mice were maintained under a 12 h light/dark cycle. Mice were genotyped using tail snips obtained from the mice at the age of weaning (~3 weeks of age). The genotyping of all mice was determined using the commercial Extract-N-Amp Plant PCR Kit (Sigma), as per the manufacturer's instructions to extract DNA from the sample tissue and to prepare samples for PCR (primers and cycling steps were obtained from The Jackson Laboratory website). The PCR product was run on a 1.7% agarose gel at 100 V for 30 min and then imaged using the UVP BioDoc-It System (Pathtech).

All treatment groups contained approximately equal numbers of male and female mice. One cohort of mice was studied through to disease end stage to obtain data on locomotor function. A second cohort of mice was culled at 24 weeks of age to collect tissues for biochemical and histological analyses. All mouse procedures were approved by the Animal Ethics Committees of The University of Melbourne and the Mental Health Research Institute and complied with guidelines from the Australian National Health and Medical Research Council.

Treatment with Cu^{II}(atsm). Cu^{II}(atsm) was synthesized as previously described (Gingras et al., 1962; Blower et al., 2003), and a suspension of the compound was prepared daily in standard suspension vehicle [SSV; 0.9% (w/v) NaCl, 0.5% (w/v) Na-carboxymethylcellulose (medium viscosity), 0.5% (v/v) benzyl alcohol, and 0.4% (v/v) Tween-80]. Cu^{II}(atsm) in SSV was administered daily to SOD1G37R mice or nontransgenic littermates by gavage, commencing at 40 d of age, at a dose of 30 mg/kg body weight/d. An equivalent volume of SSV was administered to sham-treated mice. For some experiments, mice were treated with $^{65}Cu^{II}$(atsm) synthesized as per the standard Cu^{II}(atsm) except that the initial Cu source was ^{65}CuO (Trace Sciences International). In these experiments, SOD1G37R mice were treated with $^{65}Cu^{II}$(atsm), SSV, or Cu^{II}(atsm) by daily gavage for 2 weeks commencing when they were 12 weeks old. Mice in these experiments received Cu^{II}(atsm)/$^{65}Cu^{II}$(atsm) at 30 mg/kg body weight.

hCTR1xSOD1G37R mice. The human copper transporter 1 (*hCTR1*) coding sequence was amplified from human fibroblast mRNA. The forward primer was used to introduce a Flag epitope just upstream from the start codon, and the reverse primer was located just after the stop codon. The PCR product was cloned into pCMB336 (Ke et al., 2006). A 4.1 kb PvuI/StuI fragment containing the CAG promoter, the *hCTR1* insert, and a polyA signal was purified and used at 2 ng/μl for pronuclear microinjections in C57BL/6 females (Mouseworks, Monash University, Melbourne, Victoria, Australia). hCTR1 mice were genotyped by PCR of genomic DNA isolated from ear notches (Viagen Biotech). The detection of the *hCTR1* transgene and the endogenous *mCtr1* gene (as a control for the integrity of the extracted DNA) was performed with the following primers: sense oligonucleotide *hCTR1* #1 (5′-TAAGTCACAAGTCAGCA TTCGC), corresponding to the coding sequence of the *hCTR1* transgene and the antisense oligonucleotide SP6(2) from the vector (5′-GCTCTAGCATTTAGGTGACACTATAG); the sense oligonucleotide *mCtr1* #2 (5′-GCCAAGAGACCTTTGCTCTG) and the antisense oligonucleotide *mCtr1* #3 (5′-GCACCTTAATGTTGGGCTGT), corresponding to the 3′ untranslated region of the endogenous *mCtr1* gene. C57BL/6 mice positive for the *hCTR1* transgene were backcrossed for two generations, then bother/sister mating continued for a further seven generations. Double-transgenic hCTR1xSOD1G37R mice were created by mating SOD1G37R hemizygotes with hCTR1 hemizygotes. Litters were genotyped for all possible genetic variants via PCR, as described above.

hCTR1 expression was quantified using qRT-PCR methods that were described previously (Kanninen et al., 2013) with all cDNA synthesis and qRT-PCR reagents from Life Technologies. Briefly, RNA from nontransgenic and transgenic hCTR1 mouse spinal cord tissue (5 mg) was isolated, and treated with DNase using the MagMAX-96 Total RNA Isolation Kit. RNA concentrations were quantified using the Qubit 2.0 Fluorometer, then 200 ng of RNA was reverse transcribed using the High Capacity cDNA Reverse Transcription Kit. Primers for *hCTR1* were GCTGGAAGAAGGCAGTGGTA and GGCCACGCCATAGAGTTTG, and for *mCtr1* they were TTCTTCAGGGTAGCTTCCGAGTA and CAACCTAGCGCAGGGATCT. Each 10 μl reaction mix consisted of 300 nM primers, 5 μl 2× Power SYBR Green Master Mix, and 20 ng of cDNA template. Duplicate reactions were performed using the LightCycler 480 (Roche) and the following conditions: 10 min at 95°C, followed by 45 cycles of 15 s at 95°C, and 60°C for 60 s. Cycle threshold (Ct) values were calculated as the lowest cycle number producing an exponential increase in PCR product amplification. Samples with Ct values <30 were excluded from all analyses. The ΔCt method was used to normalize *hCTR1* gene expression in each sample to the expression of endogenous *mCtr1*. To assess whether *hCTR1* expression altered the expression of endogenous *mCtr1*, the ΔCt method was used to normalize *mCtr1* gene expression in each sample to the expression of endogenous *mActb*.

Locomotor function. Mice were tested for a locomotor function using the rotarod assay. Mice were trained for 5 d before data were recorded for analysis. During the data collection phase of the study, the mice were tested on the rotarod twice a week. For SOD1G37R mice treated with Cu^{II}(atsm), the rotation speed of the rotarod was 25 rpm, and the time

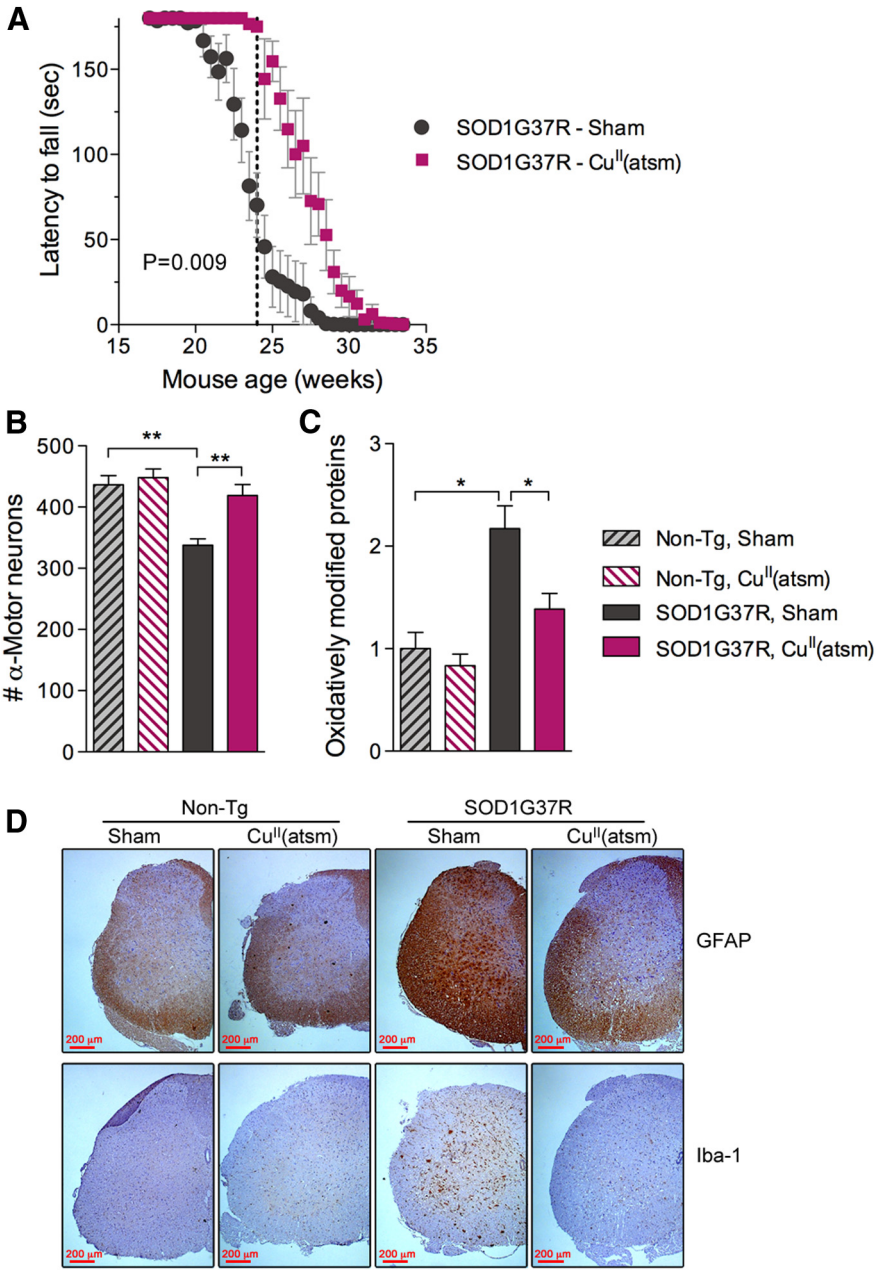

Figure 1. Effects of Cu^{II}(atsm) on locomotor function of SOD1G37R mice. ***A***, Locomotor function of SOD1G37R mice measured as latency to fall on the rotarod assay ($n = 10$ sham-treated SOD1G37R mice, $n = 6$ Cu^{II}(atsm)-treated SOD1G37R mice). The dashed line at 24 weeks represents an additional cohort of mice that was culled for all analyses shown in ***B–D*** and in Figures 2-5. The *p* value shown represents the statistical significance of the treatment effect (two-way repeated-measures ANOVA). ***B***, Number of motor neurons present in the lumbar region of spinal cords from SOD1G37R mice and nontransgenic littermates. ***C***, Abundance of oxidatively modified proteins determined using the OxyBlot assay in spinal cord tissue expressed relative to levels detected in sham-treated, nontransgenic littermate controls. ***D***, Representative histology images for GFAP (top row) and Iba-1 (bottom row) immunoreactivity in spinal cord transverse sections. Asterisks in ***B*** and ***C*** represent the statistical significance of the data as follows: $*p < 0.05$, $**p < 0.01$. $n = 4–8$ for all treatment groups for data in ***B–D***. Error bars represent the SEM.

that each mouse could no longer stay on the rotarod (latency to fall) was recorded up to a maximum of 180 s. For mice in the hCTR1xSOD1G37R study, the rotation speed of the rotarod accelerated from 4 to 40 rpm over 180 s. Mice were placed on the rotarod twice during each testing period, and only their maximum score recorded for analysis. Researchers performing the rotarod assay were blinded to the treatments.

Mouse survival. SOD1G37R mice eventually develop limb paralysis that prevents them from accessing food and water, and individual mice in this study, regardless of treatment, were culled once they reached this stage. This stage was identified as the point at which individual mice had complete paralysis in at least one hindlimb and were unable to right themselves within 15 s after being laid down on their side. All survival data presented in this study therefore represent the age at which the mice reached this disease stage. Researchers who culled mice were blinded to the treatments and mouse genotype.

Tissue collection. Mice allocated to collecting tissues for biochemical analyses were killed when 24 weeks old. These mice were killed by intraperitoneal injection of PBS supplemented with ketamine (20 mg/ml) and xylazine (4 mg/ml), followed by transcardial perfusion with PBS containing 0.25% phosphatase inhibitor mixture, 1% protease inhibitor (Roche), and 20 U/ml heparin. After perfusion, spinal cords and brains were removed. A small 5 mm section of the lumbar region of the spinal cord was removed and submersion fixed in 4% (v/v) paraformaldehyde, and a similar lumbar section was snap frozen on dry ice for subsequent mass spectrometry analyses. The remaining spinal cord material was snap frozen on dry ice for subsequent protein extraction and additional biochemical analyses.

SDS-PAGE. Spinal cords were homogenized using disposable polypropylene pestles for Microfuge tubes (USA Scientific) in PBS supplemented with protease and phosphatase inhibitors (Sigma), then PBS-soluble and PBS-insoluble fractions were collected by centrifugation (16,000 × *g*, for 30 min at 4°C). After determining the protein content via the BCA Assay (Thermo Scientific), samples were prepared in a sample buffer [62.6 mM Tris, 5% (v/v) glycerol, 2% (w/v) SDS, and 0.0025% (w/v) bromophenol blue], then were loaded onto 12% NuPAGE Novex Bis-Tris gels (Life Technologies) and electrophoresed at 175 V for 60 min in MES SDS running buffer (Life Technologies). Resolved proteins were transferred to PVDF membranes, and Western blotting was performed as described previously (Donnelly et al., 2012). The primary antibodies that were used were raised to detect human SOD1 (Abcam), mouse SOD1 (Abnova), and GAP43 (Novus Biologicals). Antibody immunoreactivity was detected using enhanced chemiluminescence (ECL Advance, GE Healthcare) and a FujiFilm LAS-3000 imager. Chemiluminescence images were saved as TIFF files, and the relative intensity of immunoreactivity was determined using NIH ImageJ version 1.38x software.

Native PAGE. PBS-soluble and PBS-insoluble spinal cord extracts generated as described above were prepared in native PAGE sample buffer [100 mM Tris, 10% (v/v) glycerol, 0.0025% (w/v) bromophenol blue, pH 8.6], then resolved on 12% tris-glycine gels (Life Technologies) at 125 V for 100 min in native tris-glycine running buffer (Life Technologies) before transferring to PVDF membranes as described above. Membranes were probed using the primary antibodies A5C3, B8H10, and C4F6 (MédiMabs). All three of these antibodies were generated to specifically detect misfolded forms of human SOD1 but not natively folded wild-type SOD1, and data supporting this conformation-dependent immunoreactivity have been presented (Bosco et al., 2010; Gros-Louis et al., 2010). Immunoreactivity for these three antibodies was detected and quantified as described above.

Histology. Histology was performed based on methods previously described (Li et al., 2006). Lumbar sections of mouse spinal cord were fixed in 4% (w/v) paraformaldehyde in PBS, then were embedded in wax and transverse 5 or 20 μm sections were collected on glass slides. The 20 μm sections were stained for nucleic acid material using cresyl violet (700 μM in dH_2O, pH 3.8, with 1% acetic acid), then α-motor neurons in the ventral horn were counted using light microscopy. Thirty-six sections from spinal cord regions spanning ~1800 μm along the longitudinal plane of the spinal cord were counted per mouse. The data presented in Figure 1*B* represent the total number of α-motor neurons counted per mouse per ventral horn. To assess the levels of Iba-1 and GFAP, 5 μm sections were quenched with peroxide, blocked with 20% (v/v) serum, then were incubated with primary antibody (1:1000) overnight at 4°C. To assess the levels of human SOD1 and misfolded forms there of proteinase-K-treated, 5 μm sections were blocked with 20% (v/v) serum then were incubated overnight at 4°C with primary antibodies to misfolded SOD1, as described above. Sections were developed using the universal LSAB+HRP kit (Dako), as described by the manufacturer.

Protein oxidation. PBS-soluble tissue extracts, prepared as described above, were analyzed for oxidatively modified proteins using the OxyBlot Protein Oxidation Detection Kit (Millipore). Oxidatively modified proteins were derivatized as per kit instructions then loaded onto 12% tris-glycine gels (Life Technologies) before transfer to PVDF membranes as described above. Membranes were probed for derivatized proteins using kit antibodies, and oxidatively modified proteins were detected via chemiluminescence as described above.

SOD activity assay. SOD activity gels were performed as previously described (Soon et al., 2011). Briefly, soluble samples collected from spinal cord tissue were diluted in native sample buffer, and 1 μg of protein was loaded onto a native 12% tris-glycine gel. After electrophoresis, gels were immersed in nitroblue tetrazolium then developed with tetramethylethylenediamine and riboflavin in KH_2PO_4 buffer.

Mass spectrometric quantification. The metal status and total SOD concentration was determined as described previously (Rhoads et al., 2011) with the following modifications. Mouse tissues were dissected and frozen on a plastic dissection plate placed on a block of dry ice to maintain a subzero temperature. For spinal cords, 1- to 2-mm-thick transverse sections were cut with a razor blade, laid flat on the dissection plate, and 0.3-mm-diameter punches of either dorsal or ventral gray matter (300 μm biopsy punch, Zivic Instruments) were obtained. The tissue was expelled with air from the punch onto a tarred aluminum weigh boat (VWR) and then weighed to the nearest microgram using an analytical balance (model 25 automatic electrobalance, Cahn). Punch weights ranged between 90 and 200 μg. The punch was then mixed with 5 μl of 10 mM ammonium acetate, pH 5.1, containing 500 nM bovine SOD as an internal standard. The supernatant was then bound to an equilibrated C_4 Ziptip (Millipore) and desalted by aspirating with 10 μl of deionized water, which was repeated six times. The point of the Ziptip was then pressed into PEEK tubing, leading to the electrospray ionization source of an LTQ-FT Ultra MS unit (Thermo Scientific) with an electrospray ionization interface in positive-ion mode. A second piece of PEEK tubing coming from the HPLC pump was inserted into the rear of the Ziptip, and the tip was then perfused with a mobile phase of 30% (v/v) acetonitrile/water with 100 μM formic acid (at 30 ml/min). The elution of SOD occurred over 2–3 min, after which time the total ion count returned to baseline. Integration and quantitation of SOD was performed as described previously (Rhoads et al., 2011, 2013).

Size exclusion chromatography inductively couple plasma mass spectrometry. Liquid chromatography coupled to inductively coupled plasma mass spectrometry (LC-ICPMS) was performed using an HPLC unit (model 1200, Agilent) equipped with binary pumps, an in-line degasser, a thermostat-controlled column compartment, a variable wavelength detector, and a temperature controlled autosampler. The HPLC was directly connected to a Teflon Mira Mist Nebulizer with PEEK tubing. An Agilent 7700 series ICPMS instrument was used as a multielemental detector and was operated in He mode (4.3 ml/min) under routine multielemental operating conditions. Samples were chromatographically separated with a BioSEC3 size exclusion column (4.6 × 300 mm, 300Å; Agilent) with 200 mM ammonium nitrate, pH 8.0, at a flow rate of 0.4 ml/min (145 cm/h, 30°C). The size exclusion column was calibrated using the following molecular weight standards, and elution volume was monitored both by absorbance (280 nm) and by ICPMS (mass of each standard, element detected by ICPMS, and source of standard are shown in parentheses): thyroglobin (667 kDa; I; GE), ferritin (440 kDa; Fe; GE), catalase (232 kDa; Fe; GE), albumin (64 kDa; Fe, Cu, Zn; GE), bovine SOD1 (32 kDa; Cu, Zn; Sigma), and vitamin B_{12} (1.2 kDa; Co; Sigma), and the integration time for each element was 0.2 s. A standard curve of SOD1 (bovine, Sigma) was also determined by measuring the amount of SOD protein (ε_{258} = 10,300 M^{-1} cm^{-1}), and the total amount of Cu and Zn was determined by bulk measure ICPMS. The standard curve was linear over the range of 1–1000 pmol SOD injected on column (r^2 >0.98). PBS-soluble spinal cord extracts (prepared as described above) containing 200 μg of total protein were injected on column (~20 μl injections) and developed for 1.6 column volumes (8 ml).

Laser ablation inductively couple plasma mass spectrometry. Laser ablation ICPMS (LA-ICPMS) imaging mass spectrometry was performed on paraformaldehyde-fixed spinal cord transverse sections, as previously described (Hare et al., 2012; Lear et al., 2012). Imaging mass spectrometry is a relatively new analytical science that combines discrete solid sampling with mass specific detection. LA-ICPMS uses high-energy laser pulses to provide a source of particles for inorganic mass spectrometry, allowing spatial profiling of trace metals directly in solid samples. Quantitative images depicting the spatial distribution of metals in tissue sections are produced by rastering the laser beam across the tissue surface.

Statistical analyses. The Kolmogorov–Smirnov test for normality (with a Dallal-Wilkinson-Lilliefor-corrected p value) was applied to all datasets to test for Gaussian distribution. Normally distributed data were analyzed using the unpaired t test when comparing the mean of two datasets or a two-way ANOVA (with Bonferroni post-tests). Data that did not fit Gaussian distribution were analyzed using the Mann–Whitney test when comparing the mean of two datasets. The statistical significance of mouse survival data was determined using the Log-rank (Mantel–Cox) test. The statistical significance of locomotor function data was determined using a two-way repeated-measures ANOVA.

Results

Cu^{II}(atsm) is protective in SOD1G37R mice

Daily treatment with Cu^{II}(atsm) improves locomotor function and survival of SOD1G37R mice in a dose-dependent manner without affecting locomotor function of nontransgenic littermates (McAllum et al., 2013; Fig. 1*A*). The observed therapeutic outcomes involve broad protection against the toxic effects of mutant SOD1 as treatment with Cu^{II}(atsm) preserved the number of α-motor neurons in the spinal cord (Fig. 1*B*), decreased levels of oxidatively modified proteins (Fig. 1*C*), decreased the abundance of GFAP-immunoreactive cells (astrocytes) within spinal cord gray matter, and decreased the abundance of activated microglia (Fig. 1*D*). All biochemical and histological analyses were performed on tissues collected at the mid-symptom age of 24 weeks, as indicated by the vertical dashed line in Figure 1*A*. Relatively modest changes in α-motor neuron numbers are consistent with the severity of disease symptoms at this age (Feeney et al., 2001).

Cu^{II}(atsm) increases levels of mutant SOD1 *in vivo* by increasing the Cu content of the protein

We examined whether therapeutic activity of Cu^{II}(atsm) was related to effects on levels of mutant SOD1. Surprisingly, an increase in the mutant form of SOD1 was detected in the spinal cords of Cu^{II}(atsm)-treated mice. This was evident via Western blot (Fig. 2*A*,*B*) and histology (Fig. 2*C*). Endogenous, wild-type mouse SOD1 was not affected by the Cu^{II}(atsm) treatment (Fig. 2*A*,*B*). A substantial pool of metal-deficient SOD1 (i.e., where each monomer equivalent of SOD1 contains one Cu ion or one Zn ion, but not both) was decreased by the Cu^{II}(atsm) treatment,

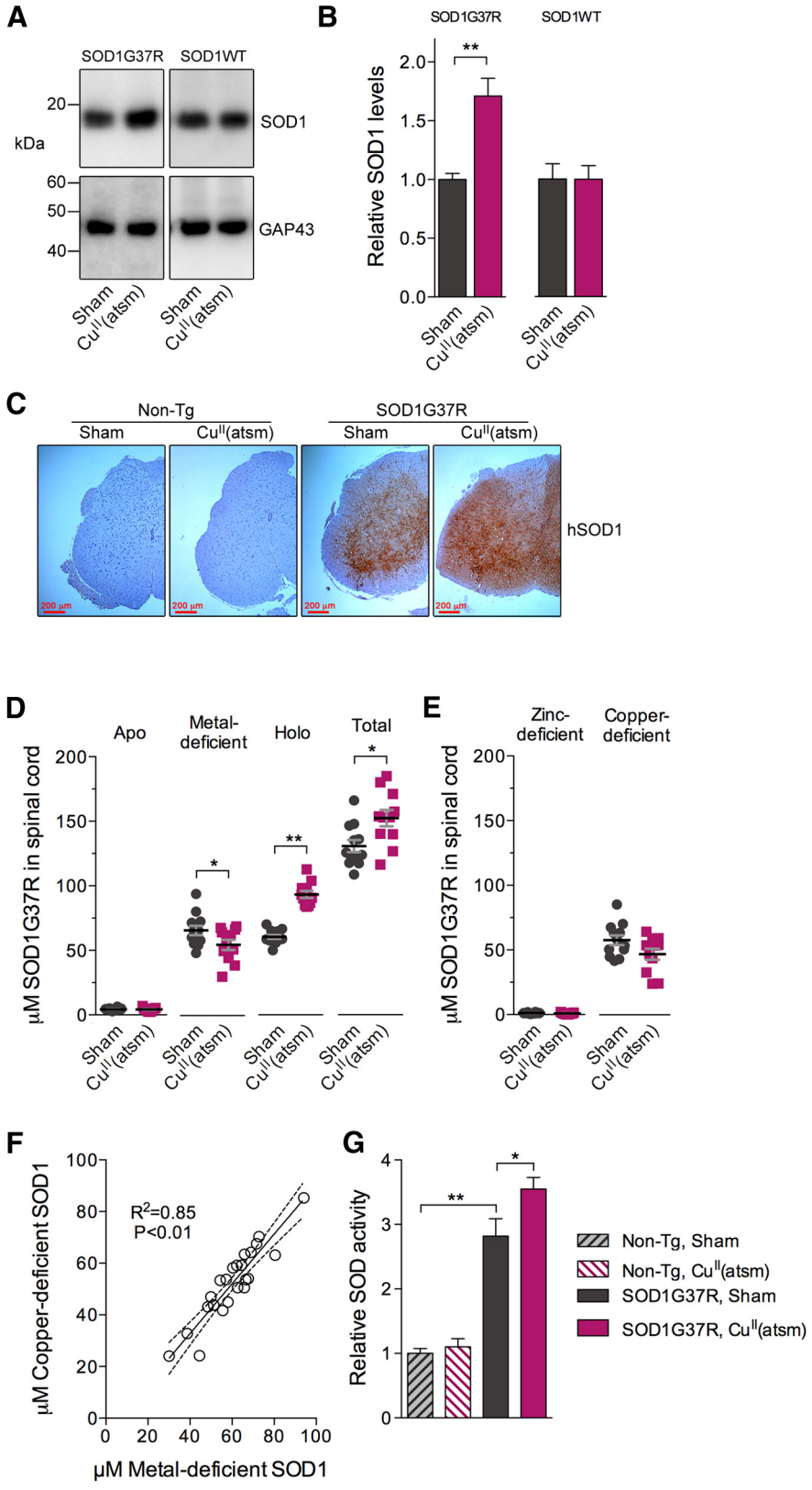

Figure 2. Effects of Cu^{II}(atsm) on SOD1G37R in the spinal cord tissue of SOD1G37R mice. ***A***, Representative Western blot images showing the effects of Cu^{II}(atsm) on levels of SOD1G37R in the spinal cords of SOD1G37R mice, and on the levels of endogenous wild-type SOD1 (SOD1WT) in nontransgenic littermates. Levels of GAP43 are shown as a loading control. ***B***, Densitometry analysis of Western blot analyses represented in ***A***. ***C***, Representative histology images for human SOD1 immunoreactivity in spinal cord transverse sections from SOD1G37R mice and nontransgenic littermates. ***D***, Mutant SOD1 in the spinal cords of SOD1G37R mice determined by mass spectrometry showing concentrations of apo, metal-deficient, and holo forms of the protein as well as the total concentration of the protein. ***E***, Concentration of zinc-deficient and copper-deficient forms of the metal-deficient pool of mutant SOD1. Note the same scale on the *y*-axes in ***D*** and ***E***. ***F***, Correlation between levels of metal-deficient SOD1 (from ***D***) and copper-deficient SOD1 (from ***E***) in the spinal cords of sham-treated and Cu^{II}(atsm)-treated SOD1G37R mice. There was no correlation between metal-deficient SOD1 and zinc-deficient SOD1 ($R^2 = 0.003$, $p = 0.8$; data not shown). ***G***, Activity of SOD in spinal cord samples expressed relative to sham-treated, nontransgenic littermate controls. Asterisks indicate the statistical significance relative to sham-treated SOD1G37R mice or as otherwise indicated: $*p < 0.05$, $**p < 0.01$. $n = 5–8$ for all treatment groups in ***A***, ***B***, and ***G***; $n = 10–11$ in ***D–F***; $n = 4$ in ***C***. Error bars represent the SEM.

whereas the increase in total SOD1 was driven by an increase in the pool of fully metallated holo-SOD1 (Fig. 2*D*). Conversion of metal-deficient SOD1 to holo-SOD1 appeared to be driven by the delivery of Cu to the mutant protein as Cu-deficient SOD1 was the only form of metal-deficient SOD1 that decreased (Fig. 2*E*), as indicated by the strong correlation between metal-deficient SOD1 and Cu-deficient SOD1 (Fig. 2*F*). There was no correlation between metal-deficient SOD1 and Zn-deficient SOD1 ($R^2 = 0.003$, $p = 0.8$; data not shown). Supporting an increase in the amount of SOD1 that contained Cu, SOD activity was increased in the spinal cords of Cu^{II}(atsm)-treated SOD1G37R mice (Fig. 2*G*).

LA-ICPMS data (Fig. 3) showed that oral treatment with Cu^{II}(atsm) increased the Cu content of the spinal cords of nontransgenic mice 2.2-fold (Fig. 3), and this is consistent with data showing that orally administered Cu^{II}(atsm) penetrates CNS tissue (Soon et al., 2011; Hung et al., 2012). The increase in spinal cord Cu was more pronounced in SOD1G37R mice (Fig. 3*B*), indicating that the Cu^{II}(atsm) had elevated penetration of CNS tissue in SOD1G37R mice or that the compound was selectively retained and/or metabolized within the CNS tissue of SOD1G37R mice. Treatment with Cu^{II}(atsm) also increased the overall levels of Zn in spinal cords of SOD1G37R mice, but, unlike Cu, the increase in Zn was not evident in nontransgenic mice (Fig. 3). Fe levels (Fig. 3) and Mn levels (data not shown) were not changed.

To gain further information on the Cu^{II}(atsm)-induced changes within the pool of holo-SOD1G37R and its associated metal ions Cu and Zn, we performed size exclusion LC-ICPMS. This metalloproteomic approach revealed that Cu and Zn were both increased in SOD1 by the Cu^{II}(atsm) treatment (Fig. 4*A*,*B*). The Cu/Zn ratio within the SOD1G37R calculated from these LC-ICPMS data con-

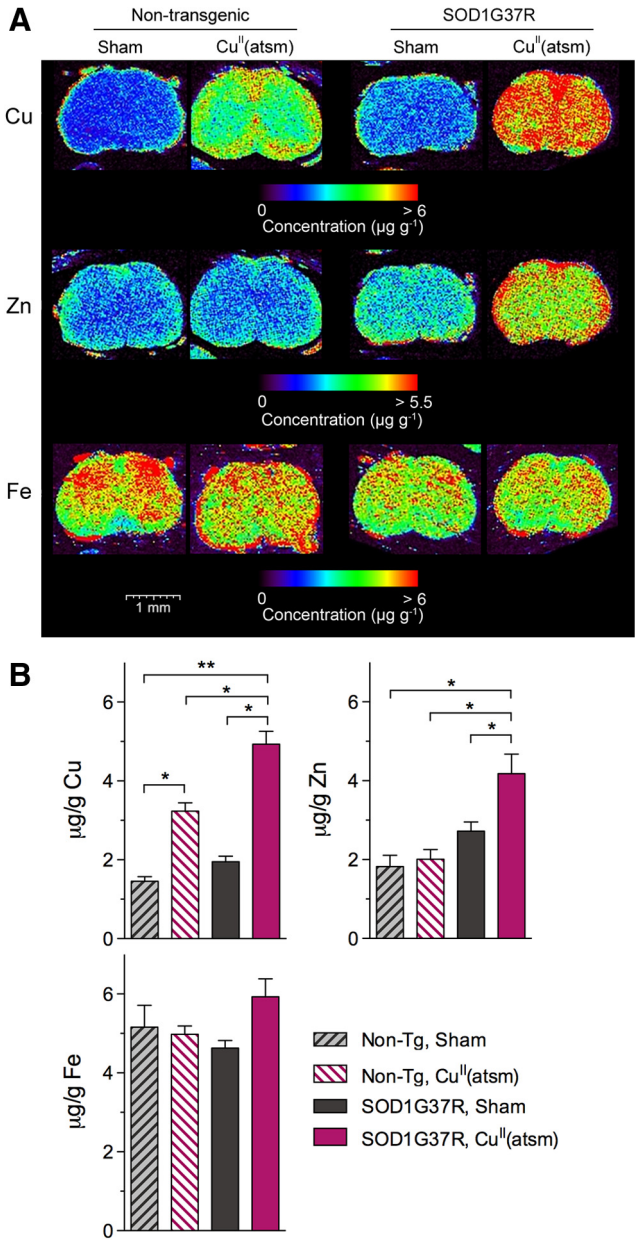

Figure 3. Metal content of spinal cord tissue from SOD1G37R mice and nontransgenic littermates. ***A***, Representative reconstructed images of LA-ICPMS data showing amounts of Cu, Zn, and Fe in spinal cord transverse sections. The pixel color represents metal ion abundance, as indicated by the spectra shown for each metal ion. ***B***, Mean data collected from LA-ICPMS analyses, as represented in ***A***. Mean data are for whole spinal cord transverse sections and therefore include apparent regionalized differences in signal intensity. Asterisks indicate statistical significance, as indicated: *$p < 0.05$, **$p < 0.01$. $n = 4$ for all treatment groups. Error bars represent the SEM.

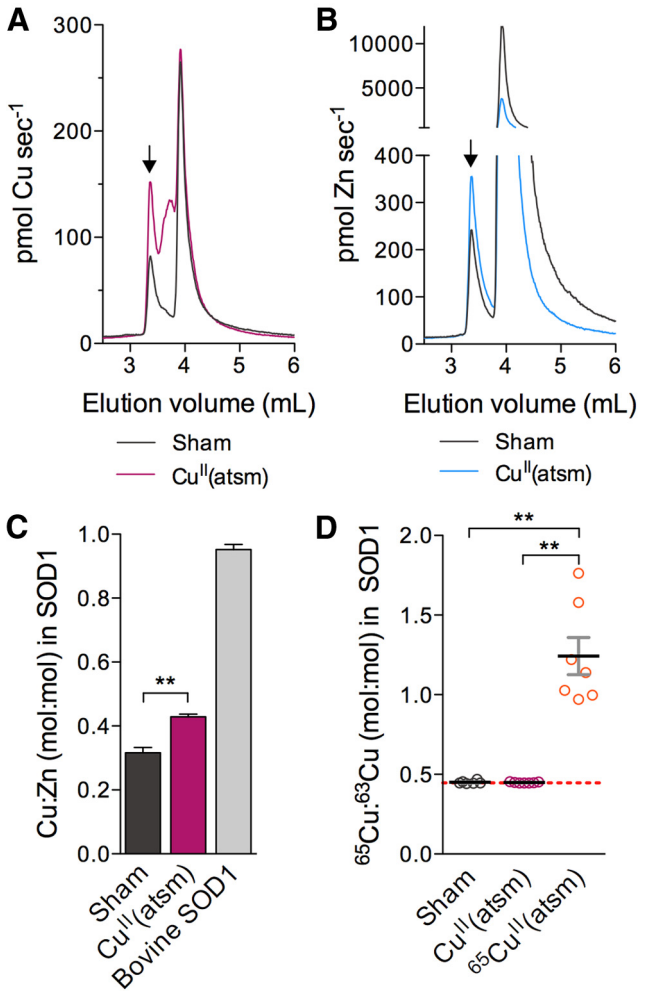

Figure 4. Effects of Cu^{II}(atsm) on the metal content of SOD1 in spinal cords of SOD1G37R mice. ***A***, Mean LC-ICPMS traces showing the effects of Cu^{II}(atsm) on Cu content of SOD1 in spinal cords of SOD1G37R mice. ***B***, Mean LC-ICPMS traces showing the effects of Cu^{II}(atsm) on the Zn content of SOD1 in spinal cords of SOD1G37R mice. SOD1 eluted at 3.4 ml is indicated by a vertical arrow in ***A*** and ***B***. ***C***, Mean data derived from SOD1 peak in ***A*** and ***B***, showing the effects of Cu^{II}(atsm) on the molar Cu/Zn ratio in SOD1 from the spinal cords of SOD1G37R mice. The Cu/Zn ratio in purified bovine SOD1 is shown as a control. ***D***, Molar ^{65}Cu/^{63}Cu ratio in SOD1 from the spinal cords of sham-, Cu^{II}(atsm)-, and ^{65}Cu^{II}(atsm)-treated SOD1G37R mice determined by LC-ICPMS, as in ***A*** and ***B***. The horizontal red dashed line shows the natural isotopic distribution of the ^{65}Cu/^{63}Cu ratio in biological material (0.45:1). Values above this line indicate an increase in the relative amount of ^{65}Cu in the SOD1. Asterisks indicate the statistical significance (**$p < 0.01$). $n = 6–7$ for all treatment groups, except for the bovine SOD1 standard in ***C***, where $n = 4$. Symbols in ***D*** represent data for individual mice. Error bars represent the SEM.

firmed that SOD1G37R in the spinal cords of vehicle-treated mice was relatively Cu deficient (Fig. 4*C*). The Cu^{II}(atsm)-induced increase in the SOD1G37R Cu/Zn ratio was consistent with the LA-ICPMS data (Fig. 3), which showed that Cu^{II}(atsm) had a greater effect on Cu levels in the spinal cord compared with Zn.

Data in Figures 3 and 4 collectively indicate that treatment with Cu^{II}(atsm) increases the total levels of Cu and Zn and the amount of holo-mutant SOD1 within the spinal cord tissue. Cu^{II}(atsm) has the capacity to increase levels of bioavailable Cu and Zn in cells *in vitro* (Donnelly et al., 2012). This indicates that the increase in Cu in the mutant SOD1 (Fig. 4*A*) involved the transfer of Cu from Cu^{II}(atsm) to SOD1, and that the increase in Zn occurs via an indirect mechanism. To probe further the *in vivo* transfer of Cu from Cu^{II}(atsm) to mutant SOD1, mice were treated with Cu^{II}(atsm) isotopically enriched with ^{65}Cu. This naturally occurring isotope is less abundant than the predominant ^{63}Cu isotope, with the natural ratio of 0.45:1 (^{65}Cu/^{63}Cu). LC-ICPMS analysis of spinal cord tissue demonstrated an increase in abundance of ^{65}Cu in the SOD1 of ^{65}Cu^{II}(atsm)-treated mice (Fig. 4*D*), indicating a transfer of Cu from Cu^{II}(atsm) to the SOD1. Based on a total spinal cord wet weight of ~50 mg, the data in Figure 4*D* equate to ~2% of the total Cu delivered orally to the mice as Cu^{II}(atsm) was being transferred to SOD1 in the spinal cord.

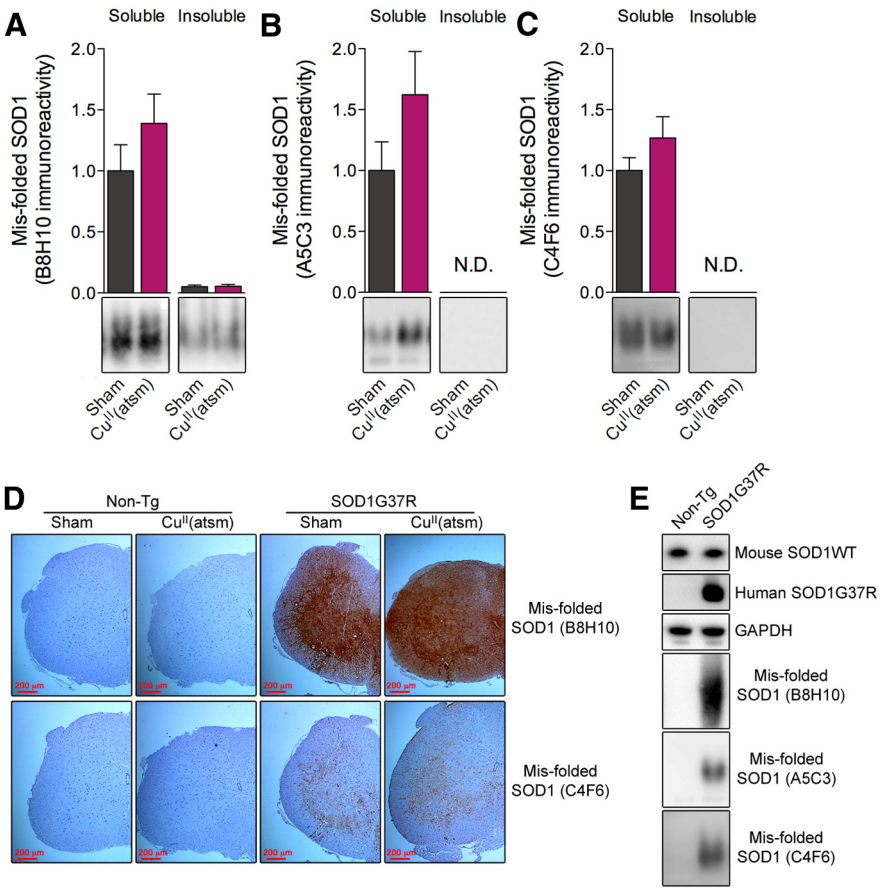

Figure 5. Misfolded SOD1 in spinal cords of SOD1G37R mice. ***A–C***, Levels of misfolded mutant SOD1 in PBS-soluble and PBS-insoluble fractions of SOD1G37R mouse spinal cords detected using native PAGE and the B8H10 (***A***), A5C3 (***B***), and C4F6 (***C***) antibodies. Values are derived from densitometry analysis of Western images (representative images shown) and are expressed relative to the immunoreactivity detected in the soluble fraction of sham-treated mice. N.D., nondetectable levels in the insoluble fraction using these antibodies. ***D***, Representative histology images for misfolded SOD1 immunoreactivity in spinal cord transverse sections using the B8H10 antibody (top row) and the C4F6 antibody (bottom row). Immunoreactivity using the A5C3 antibody was not detected by histology (data not shown). ***E***, Immunoreactivity for the three antibodies was not detected in nontransgenic mice, indicating specificity for the human mutant form of the protein. $n = 4–5$ for all treatment groups. Error bars in ***A–C*** represent the SEM.

Treatment with Cu^{II}(atsm) did not decrease levels of misfolded SOD1

Suboptimal metal content of SOD1 can promote SOD1 misfolding and aggregation (Lynch et al., 2004; Rumfeldt et al., 2009; Ip et al., 2011), and misfolded and aggregated SOD1 is a consistent feature of ALS (Bruijn et al., 1998; Furukawa et al., 2006; Wang et al., 2008; Chattopadhyay and Valentine, 2009; Prudencio et al., 2009), including sporadic ALS (Bosco et al., 2010). Given that Cu^{II}(atsm) improved the metal content of the mutant SOD1 (Fig. 3), the levels of misfolded SOD1 in the spinal cords of Cu^{II}(atsm)-treated SOD1G37R mice were assessed using three antibodies raised against misfolded SOD1 (Bosco et al., 2010; Gros-Louis et al., 2010). Misfolded SOD1 was readily detectable in the soluble fraction of spinal cords from SOD1G37R mice, but the Cu^{II}(atsm) treatment did not significantly alter its abundance (Fig. 5*A–C*). The results for all three antibodies trended toward an increase in misfolded SOD1 in the soluble fraction in the Cu^{II}(atsm)-treated mice, and this was supported by histology data (Fig. 5*D*). Consistent with previous reports (Rakhit et al., 2007; Zetterström et al., 2007; Brotherton et al., 2012), levels of misfolded SOD1 were low or nondetectable in the insoluble fraction (Fig. 5*A–C*).

Increasing spinal cord Cu via the Cu uptake transporter CTR1 improved the survival of SOD1G37R mice

To help assess the significance of Cu delivery in the protective activity of Cu^{II}(atsm) in SOD1G37R mice, we aimed to increase spinal cord Cu levels via an alternate method. This was achieved by crossing SOD1G37R mice with mice that express the gene for the human Cu uptake transporter CTR1. The expression of *hCTR1* in the spinal cord tissue (Fig. 6*A*) induced a 19% increase in spinal cord Cu levels without altering levels of Zn or Fe (Fig. 6*B*). Expression of endogenous *mCtr1* was not altered by the expression of *hCTR1* (Fig. 6*A*). The elevation in spinal cord Cu levels translated into a modest (but statistically insignificant) improvement in locomotor function (Fig. 6*C*) and a significant ($p = 0.006$) 12% increase in the median survival time of SOD1G37R mice (Fig. 6*D*).

Discussion

Early studies showed that higher levels of expressed mutant SOD1 correlate with more rapid onset and progression of disease symptoms in the ALS model mice (Gurney et al., 1994; Wong et al., 1995; Dal Canto and Gurney, 1997). This correlation is substantiated by delayed symptoms in ALS mice due to decreased mutant SOD1 levels (Ralph et al., 2005; Urushitani et al., 2007; Henriques et al., 2010). Because of this clear apparent relationship between mutant SOD1 levels and the phenotype of the mice, we measured SOD1 in the spinal cords of Cu^{II}(atsm)-treated SOD1G37R mice. Despite the fact that Cu^{II}(atsm) treatment improved mouse locomotor function and survival (McAllum et al., 2013; Fig. 1*A*), we found that it significantly increased the mutant protein *in vivo* (Fig. 2), thereby disproving the assertion that the phenotype of mutant SOD1 mice is proportional to levels of the mutant protein.

Mass spectrometry analyses indicated that Cu^{II}(atsm) promoted conversion of metal-deficient SOD1 to holo-SOD1 (Fig. 2*D–F*) via *in vivo* transfer of Cu from Cu^{II}(atsm) to the mutant SOD1; the Cu content of SOD1 was increased (Fig. 4*A*) and ^{65}Cu from orally administered $^{65}Cu^{II}$(atsm) was recovered in spinal cord SOD1 (Fig. 4*D*). These outcomes are consistent with the high stability of holo-SOD1 (Forman and Fridovich, 1973), regardless of the presence of ALS-associated mutations (Banci et al., 2007), and support the findings of *in vitro* studies that indicate SOD1 toxicity can be prevented by improving the metallation state of the protein (Estévez et al., 1999). These outcomes indicate that the metal content of SOD1 may be a greater determinant of the toxicity of the protein in mutant SOD1-associated forms of ALS than the mutations themselves.

A number of mechanisms have been proposed to explain how an altered metal content of SOD1 may cause ALS. One of these involves pro-oxidant gain of function for Zn-deficient SOD1

(Crow et al., 1997). This proposed toxic gain of function requires the retention of Cu in Zn-deficient SOD1, as it is the redox activity of Cu that catalyzes the production of reactive oxygen and nitrogen species (Crow et al., 1997; Estévez et al., 1999; Sahawneh et al., 2010). This toxic mechanism of action is supported by a number of lines of evidence (Estévez et al., 1999; Roberts et al., 2007; Sahawneh et al., 2010), and although the Zn-deficient pool of SOD1 accounts for only <1% of SOD1 in the SOD1G37R (Fig. 2*E*), our data show that the concentration of Zn-deficient SOD1 in spinal cord tissue is higher than concentrations that induce motor neuron toxicity *in vitro* (Sahawneh et al., 2010). However, SOD1 mice in which all four Cu-coordinating histidine residues in the mutant SOD1 are removed have been developed, and these mice still develop ALS-like symptoms (Wang et al., 2003). While the phenotype of these "quad mutant" mice does not exclude the Cu-mediated SOD1 toxicity occurring via Cu that binds to the SOD1 Zn-binding site (Valentine et al., 1979), the absence of any significant changes to the pool of Zn-deficient SOD1 in Cu^{II}(atsm)-treated SOD1G37R mice indicates that the modulation of Zn-deficient SOD1 is not part of the therapeutic mechanism of action for Cu^{II}(atsm).

Metal-free (apo) SOD1 readily misfolds and aggregates (Arnesano et al., 2004; Lynch et al., 2004; Furukawa et al., 2008; Durazo et al., 2009; Rumfeldt et al., 2009; Tiwari et al., 2009), thus potentially giving rise to the SOD1 aggregates present in some forms of ALS. Significantly, ALS-causing SOD1 mutations promote SOD1 misfolding via a pathway in which the mutant SOD1 preferentially loses Cu (Ip et al., 2011), and restoration of the full metal compliment of the protein makes it relatively indistinguishable from holo wild-type SOD1 (Banci et al., 2007). However, despite this relationship between Cu deficiency and SOD1 misfolding, preventing the formation of misfolded SOD1 is not the mechanism through which Cu^{II}(atsm) improved the locomotor function and survival of SOD1G37R mice, as none of the antibodies used to assess the levels of misfolded SOD1 revealed a decrease in the pool of misfolded SOD1 (Fig. 5*A–D*). In fact, all three antibodies indicated that the soluble pool of misfolded SOD1 increased in equilibrium with the total pool of SOD1 (Fig. 2*A*). Previous studies have shown that decreasing the levels of misfolded SOD1 improves the survival and locomotor function of mutant SOD1 mice, suppresses inflammatory responses, and protects spinal cord motor neurons (Gros-Louis et al., 2010; Liu et al., 2012), outcomes that were all detected in Cu^{II}(atsm)-treated SOD1G37R mice (Fig. 1). Without precluding the potential contribution of methodological differences between the studies, these apparent disparate outcomes may indicate that SOD1-mediated dysfunction in ALS is not due to a single toxic species of SOD1, and that misfolded SOD1 contributes only partially to the decreased neuron functionality in ALS. Supporting this, none of the therapeutic interventions tested to

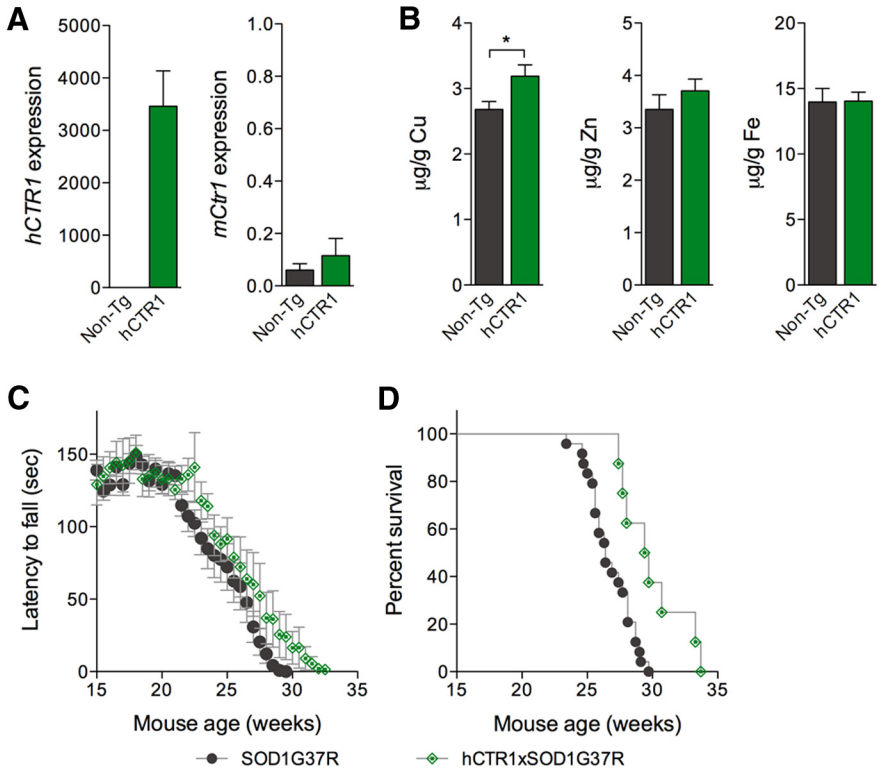

Figure 6. Effects of expressed *hCTR1* on the locomotor function and survival of SOD1G37R mice. ***A***, Levels of mRNA for *hCTR1* and *mCtr1* in the spinal cords of hCTR1 mice and nontransgenic (non-Tg) littermates. *hCTR1* levels are expressed relative to levels of the endogenous *mCtr1*, and levels of *mCtr1* are expressed relative to levels of endogenous *mActb*. ***B***, Copper, zinc, and iron content of spinal cord tissue from mice expressing *hCTR1* compared with nontransgenic littermates, as determined using LA-ICPMS as in Figure 3. $n = 6$ for both genotypes in ***A*** and ***B***. ***C***, Locomotor function of SOD1G37R and hCTR1xSOD1G37R mice measured as the latency to fall on the rotarod assay ($n = 14$ SOD1G37R mice, $n = 8$ hCTR1xSOD1G37R mice). ***D***, Fraction of SOD1G37R and hCTR1xSOD1G37R mice alive relative to age ($n = 24$ SOD1G37R mice, $n = 8$ hCTR1xSOD1G37R mice). Regardless of genotype, mice were culled when complete paralysis was present in at least one hindlimb and were unable to right themselves within 15 s after being laid down on their side. Asterisks indicate the statistical significance (*$p < 0.05$). Error bars represent the SEM.

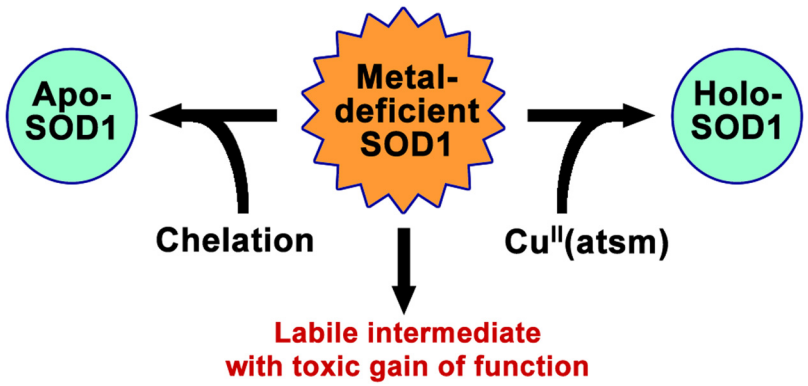

Figure 7. Schematic to indicate how both chelation and supplementation therapeutic strategies can attenuate SOD1 toxicity. Apo- and holo-SOD1 are nontoxic; apo-SOD1 is rapidly turned over, whereas holo-SOD1 is the stable, functional antioxidant form. Toxicity of the labile, metal-deficient intermediate can be prevented by chelating agents that convert holo-SOD1 to apo-SOD1, or by agents such as Cu^{II}(atsm), which convert apo-SOD1 to holo-SOD1.

date, including Cu^{II}(atsm), has completely prevented death or locomotor deficits in ALS model mice.

SOD1 that is relatively Cu deficient and Zn replete has been reported in the spinal cords of ALS model mice (Lelie et al., 2011) and is supported by data shown in Figure 4*C*. Our observation that Cu-deficient SOD1 was the only pool of SOD1 decreased by Cu^{II}(atsm) indicates that if the phenotype of the SOD1G37R mice is driven solely by mutant SOD1, increasing bioavailable Cu in the spinal cord is beneficial because it decreases the abundance of the Cu-deficient pool of SOD1. This is supported by data showing that the overexpression of CTR1 improves the survival of SOD1G37R mice (Fig. 6), and by data showing that Cu administered orally as Cu^{II}(atsm) is recovered in spinal cord SOD1 (Fig. 4*D*). However, modulating the levels of spinal cord Cu to treat mutant SOD1 mice has been investigated previously, and the outcomes often indicate that decreasing Cu is beneficial. Treatment with ammonium tetrathiomolybdate, for example, is effective in mutant SOD1 mice via a mechanism proposed to involve attenuation of the Cu dyshomeostasis caused by mutant SOD1, and is supported by data that show the treatment decreases the levels of spinal cord Cu and removes Cu from the SOD1 active site (Tokuda et al., 2008, 2013). Conversely, treating mutant SOD1 rats with pyrrolidine dithiocarbamate, a compound capable of increasing Cu levels in CNS tissue (Malm et al., 2007), accelerated the ALS-like phenotype of mutant SOD1 rats (Ahtoniemi et al., 2007). Targeting metal ion homeostasis, therefore, has good *in vivo* support as a strategy for treating ALS, but the interpretation of outcomes from studies that use notional metal-chelating agents, as opposed to metal delivery agents, is complicated by an incomplete understanding of the activity of these compounds at the cellular level, as was recently reviewed (Crouch and Barnham, 2012).

Other studies have attempted to modulate disease symptoms in mutant SOD1 mice by genetic modification of Cu transporters and chaperones. The first of these studies used mice that had no Cu chaperone for SOD1 (CCS), a cellular chaperone that delivers intracellular Cu to SOD1. The SOD1/$CCS^{-/-}$ mice had decreased Cu levels in SOD1 but did not have an altered phenotype, thus generating the conclusion that the Cu content of mutant SOD1 did not contribute to SOD1 toxicity *in vivo* (Subramaniam et al., 2002). This interpretation has been criticized (Beckman et al., 2002; Kiaei et al., 2004) based on data that show CCS is not the only chaperone that delivers Cu to SOD1 (Carroll et al., 2004). By contrast, mice that express mutant SOD1 and a dysfunctional Cu-transporting ATPase 1 (ATP7A) displayed increased survival and locomotor function relative to mutant SOD1 mice with functional ATP7A, and it was shown that the expression of the dysfunctional ATP7A significantly decreased global levels of spinal cord Cu (Kiaei et al., 2004). Also, the overexpression of CCS in mutant SOD1 mice dramatically accelerates disease onset and premature death (Son et al., 2007). Data from the CTR1-overexpressing mice (Fig. 6) support the outcomes from our Cu^{II}(atsm) studies, but on face value appear to oppose outcomes from mice with altered CCS or ATP7A functionality. Fundamental differences between the Cu transporters and chaperones modulated in these studies and their likely differing effects with respect to metallo-proteins other than SOD1 will have contributed to these apparent opposing outcomes. If anything, these studies demonstrate the often underestimated complexity of biometal metabolism. More information on how the metal content of SOD1 and other cupro-proteins is changed in these models is needed to reconcile these disparate outcomes.

While the definitive roles for altered Cu and Zn homeostasis in the toxic gain of function of SOD1 continue to be debated, the suboptimal metal content of SOD1 is nonetheless emerging as an important factor with excellent potential for therapeutic intervention. Our data indicate that Cu^{II}(atsm) may mediate its protective effects, at least in part, by delivering Cu to Cu-deficient SOD1, thereby converting it to stable, nontoxic holo-SOD1. This therapeutic strategy does not preclude the potential benefits of removing Cu from, for example, Zn-deficient SOD1 to prevent a pro-oxidant gain of function. When considered with outcomes from previous studies, our data support the conclusion that at least part of the toxic gain of function of SOD1 resides in a metal-deficient intermediate, and that driving the protein toward holo-SOD1 via metal delivery or toward apo-SOD1 via sequestration appears to have comparable therapeutic potential (Fig. 7). Our data add support to the strengthening hypothesis that combination therapy is likely to provide the best outcomes for patients with ALS.

References

Ahtoniemi T, Goldsteins G, Keksa-Goldsteine V, Malm T, Kanninen K, Salminen A, Koistinaho J (2007) Pyrrolidine dithiocarbamate inhibits induction of immunoproteasome and decreases survival in a rat model of amyotrophic lateral sclerosis. Mol Pharmacol 71:30–37. CrossRef Medline

Andersen PM, Sims KB, Xin WW, Kiely R, O'Neill G, Ravits J, Pioro E, Harati Y, Brower RD, Levine JS, Heinicke HU, Seltzer W, Boss M, Brown RH Jr (2003) Sixteen novel mutations in the Cu/Zn superoxide dismutase gene in amyotrophic lateral sclerosis: a decade of discoveries, defects and disputes. Amyotroph Lateral Scler Other Motor Neuron Disord 4:62–73. CrossRef Medline

Arnesano F, Banci L, Bertini I, Martinelli M, Furukawa Y, O'Halloran TV (2004) The unusually stable quaternary structure of human Cu, Zn-superoxide dismutase 1 is controlled by both metal occupancy and disulfide status. J Biol Chem 279:47998–48003. CrossRef Medline

Banci L, Bertini I, D'Amelio N, Libralesso E, Turano P, Valentine JS (2007) Metalation of the amyotrophic lateral sclerosis mutant glycine 37 to arginine superoxide dismutase (SOD1) apoprotein restores its structural and dynamical properties in solution to those of metalated wild-type SOD1. Biochemistry 46:9953–9962. CrossRef Medline

Beckman JS, Esétvez AG, Barbeito L, Crow JP (2002) CCS knockout mice establish an alternative source of copper for SOD in ALS. Free Radic Biol Med 33:1433–1435. CrossRef Medline

Bensimon G, Lacomblez L, Meininger V (1994) A controlled trial of riluzole in amyotrophic lateral sclerosis. ALS/Riluzole Study Group. N Engl J Med 330:585–591. CrossRef Medline

Blower PJ, Castle TC, Cowley AR, Dilworth JR, Donnelly PS, Labisbal E, Sowrey FE, Teat SJ, Went MJ (2003) Structural trends in copper(II) bis(thiosemicarbazone) radiopharmaceuticals. Dalton Trans 4416–4425. CrossRef

Bosco DA, Morfini G, Karabacak NM, Song Y, Gros-Louis F, Pasinelli P, Goolsby H, Fontaine BA, Lemay N, McKenna-Yasek D, Frosch MP, Agar JN, Julien JP, Brady ST, Brown RH Jr (2010) Wild-type and mutant SOD1 share an aberrant conformation and a common pathogenic pathway in ALS. Nat Neurosci 13:1396–1403. CrossRef Medline

Brotherton TE, Li Y, Cooper D, Gearing M, Julien JP, Rothstein JD, Boylan K, Glass JD (2012) Localization of a toxic form of superoxide dismutase 1 protein to pathologically affected tissues in familial ALS. Proc Natl Acad Sci U S A 109:5505–5510. CrossRef Medline

Bruijn LI, Houseweart MK, Kato S, Anderson KL, Anderson SD, Ohama E, Reaume AG, Scott RW, Cleveland DW (1998) Aggregation and motor neuron toxicity of an ALS-linked SOD1 mutant independent from wild-type SOD1. Science 281:1851–1854. CrossRef Medline

Carroll MC, Girouard JB, Ulloa JL, Subramaniam JR, Wong PC, Valentine JS, Culotta VC (2004) Mechanisms for activating Cu- and Zn-containing superoxide dismutase in the absence of the CCS Cu chaperone. Proc Natl Acad Sci U S A 101:5964–5969. CrossRef Medline

Chattopadhyay M, Valentine JS (2009) Aggregation of copper-zinc superoxide dismutase in familial and sporadic ALS. Antioxid Redox Signal 11:1603–1614. CrossRef Medline

Crouch PJ, Barnham KJ (2012) Therapeutic redistribution of metal ions to

treat Alzheimer's disease. Acc Chem Res 45:1604–1611. CrossRef Medline

Crow JP, Sampson JB, Zhuang Y, Thompson JA, Beckman JS (1997) Decreased zinc affinity of amyotrophic lateral sclerosis-associated superoxide dismutase mutants leads to enhanced catalysis of tyrosine nitration by peroxynitrite. J Neurochem 69:1936–1944. CrossRef Medline

Dal Canto MC, Gurney ME (1997) A low expressor line of transgenic mice carrying a mutant human Cu, Zn superoxide dismutase (SOD1) gene develops pathological changes that most closely resemble those in human amyotrophic lateral sclerosis. Acta Neuropathol 93:537–550. CrossRef Medline

DeJesus-Hernandez M, Mackenzie IR, Boeve BF, Boxer AL, Baker M, Rutherford NJ, Nicholson AM, Finch NA, Flynn H, Adamson J, Kouri N, Wojtas A, Sengdy P, Hsiung GY, Karydas A, Seeley WW, Josephs KA, Coppola G, Geschwind DH, Wszolek ZK, et al. (2011) Expanded GGGGCC hexanucleotide repeat in noncoding region of C9ORF72 causes chromosome 9p-linked FTD and ALS. Neuron 72:245–256. CrossRef Medline

Donnelly PS, Liddell JR, Lim S, Paterson BM, Cater MA, Savva MS, Mot AI, James JL, Trounce IA, White AR, Crouch PJ (2012) An impaired mitochondrial electron transport chain increases retention of the hypoxia imaging agent diacetylbis(4-methylthiosemicarbazonato)copperII. Proc Natl Acad Sci U S A 109:47–52. CrossRef Medline

Durazo A, Shaw BF, Chattopadhyay M, Faull KF, Nersissian AM, Valentine JS, Whitelegge JP (2009) Metal-free superoxide dismutase-1 and three different amyotrophic lateral sclerosis variants share a similar partially unfolded beta-barrel at physiological temperature. J Biol Chem 284:34382–34389. CrossRef Medline

Estévez AG, Crow JP, Sampson JB, Reiter C, Zhuang Y, Richardson GJ, Tarpey MM, Barbeito L, Beckman JS (1999) Induction of nitric oxide-dependent apoptosis in motor neurons by zinc-deficient superoxide dismutase. Science 286:2498–2500. CrossRef Medline

Feeney SJ, McKelvie PA, Austin L, Jean-Francois MJ, Kapsa R, Tombs SM, Byrne E (2001) Presymptomatic motor neuron loss and reactive astrocytosis in the SOD1 mouse model of amyotrophic lateral sclerosis. Muscle Nerve 24:1510–1519. CrossRef Medline

Forman HJ, Fridovich I (1973) On the stability of bovine superoxide dismutase. The effects of metals. J Biol Chem 248:2645–2649. Medline

Furukawa Y, Fu R, Deng HX, Siddique T, O'Halloran TV (2006) Disulfide cross-linked protein represents a significant fraction of ALS-associated Cu, Zn-superoxide dismutase aggregates in spinal cords of model mice. Proc Natl Acad Sci U S A 103:7148–7153. CrossRef Medline

Furukawa Y, Kaneko K, Yamanaka K, O'Halloran TV, Nukina N (2008) Complete loss of post-translational modifications triggers fibrillar aggregation of SOD1 in the familial form of amyotrophic lateral sclerosis. J Biol Chem 283:24167–24176. CrossRef Medline

Gingras BA, Suprunchuk T, Bayley CH (1962) The preparation of some thiosemicarbazones and their copper complexes: part III. Can J Chem 40:1053–1059. CrossRef

Graffmo KS, Forsberg K, Bergh J, Birve A, Zetterström P, Andersen PM, Marklund SL, Brännström T (2013) Expression of wild-type human superoxide dismutase-1 in mice causes amyotrophic lateral sclerosis. Hum Mol Genet 22:51–60. CrossRef Medline

Gros-Louis F, Soucy G, Larivière R, Julien JP (2010) Intracerebroventricular infusion of monoclonal antibody or its derived Fab fragment against misfolded forms of SOD1 mutant delays mortality in a mouse model of ALS. J Neurochem 113:1188–1199. CrossRef Medline

Gurney ME, Pu H, Chiu AY, Dal Canto MC, Polchow CY, Alexander DD, Caliendo J, Hentati A, Kwon YW, Deng HX (1994) Motor neuron degeneration in mice that express a human Cu, Zn superoxide dismutase mutation. Science 264:1772–1775. CrossRef Medline

Hare D, Austin C, Doble P (2012) Quantification strategies for elemental imaging of biological samples using laser ablation-inductively coupled plasma-mass spectrometry. Analyst 137:1527–1537. CrossRef Medline

Henriques A, Pitzer C, Schneider A (2010) Characterization of a novel SOD-1(G93A) transgenic mouse line with very decelerated disease development. PLoS One 5:e15445. CrossRef Medline

Hung LW, Villemagne VL, Cheng L, Sherratt NA, Ayton S, White AR, Crouch PJ, Lim S, Leong SL, Wilkins S, George J, Roberts BR, Pham CL, Liu X, Chiu FC, Shackleford DM, Powell AK, Masters CL, Bush AI, O'Keefe G, et al. (2012) The hypoxia imaging agent CuII(atsm) is neuroprotective and improves motor and cognitive functions in multiple animal models of Parkinson's disease. J Exp Med 209:837–854. CrossRef Medline

Ip P, Mulligan VK, Chakrabartty A (2011) ALS-causing SOD1 mutations promote production of copper-deficient misfolded species. J Mol Biol 409:839–852. CrossRef Medline

Kanninen KM, Grubman A, Caragounis A, Duncan C, Parker SJ, Lidgerwood GE, Volitakis I, Ganio G, Crouch PJ, White AR (2013) Altered biometal homeostasis is associated with CLN6 mRNA loss in mouse neuronal ceroid lipofuscinosis. Biol Open 2:635–646. CrossRef Medline

Ke BX, Llanos RM, Wright M, Deal Y, Mercer JF (2006) Alteration of copper physiology in mice overexpressing the human Menkes protein ATP7A. Am J Physiol Regul Integr Comp Physiol 290:R1460–R1467. CrossRef Medline

Kiaei M, Bush AI, Morrison BM, Morrison JH, Cherny RA, Volitakis I, Beal MF, Gordon JW (2004) Genetically decreased spinal cord copper concentration prolongs life in a transgenic mouse model of amyotrophic lateral sclerosis. J Neurosci 24:7945–7950. CrossRef Medline

Lacomblez L, Bensimon G, Leigh PN, Guillet P, Meininger V (1996) Dose-ranging study of riluzole in amyotrophic lateral sclerosis. Amyotrophic Lateral Sclerosis/Riluzole Study Group II. Lancet 347:1425–1431. CrossRef Medline

Lear J, Hare DJ, Fryer F, Adlard PA, Finkelstein DI, Doble PA (2012) High-resolution elemental bioimaging of Ca, Mn, Fe, Co, Cu, and Zn employing LA-ICP-MS and hydrogen reaction gas. Anal Chem 84:6707–6714. CrossRef Medline

Lelie HL, Liba A, Bourassa MW, Chattopadhyay M, Chan PK, Gralla EB, Miller LM, Borchelt DR, Valentine JS, Whitelegge JP (2011) Copper and zinc metallation status of copper-zinc superoxide dismutase from amyotrophic lateral sclerosis transgenic mice. J Biol Chem 286:2795–2806. CrossRef Medline

Li QX, Mok SS, Laughton KM, McLean CA, Volitakis I, Cherny RA, Cheung NS, White AR, Masters CL (2006) Overexpression of Abeta is associated with acceleration of onset of motor impairment and superoxide dismutase 1 aggregation in an amyotrophic lateral sclerosis mouse model. Aging Cell 5:153–165. CrossRef Medline

Liu HN, Tjostheim S, Dasilva K, Taylor D, Zhao B, Rakhit R, Brown M, Chakrabartty A, McLaurin J, Robertson J (2012) Targeting of monomer/misfolded SOD1 as a therapeutic strategy for amyotrophic lateral sclerosis. J Neurosci 32:8791–8799. CrossRef Medline

Lynch SM, Boswell SA, Colón W (2004) Kinetic stability of Cu/Zn superoxide dismutase is dependent on its metal ligands: implications for ALS. Biochemistry 43:16525–16531. CrossRef Medline

Malm TM, Iivonen H, Goldsteins G, Keksa-Goldsteine V, Ahtoniemi T, Kanninen K, Salminen A, Auriola S, Van Groen T, Tanila H, Koistinaho J (2007) Pyrrolidine dithiocarbamate activates Akt and improves spatial learning in APP/PS1 mice without affecting beta-amyloid burden. J Neurosci 27:3712–3721. CrossRef Medline

McAllum EJ, Lim NKH, Hickey JL, Paterson BM, Donnelly PS, Li QX, Barnham KJ, White AR, Crouch PJ (2013) Therapeutic effects of Cu^{II}(atsm) in the SOD1G37R mouse model of amyotrophic lateral sclerosis. Amyotroph Lateral Scler Fronto Degen 14:586–590. CrossRef

Miller RG, Bouchard JP, Duquette P, Eisen A, Gelinas D, Harati Y, Munsat TL, Powe L, Rothstein J, Salzman P, Sufit RL (1996) Clinical trials of riluzole in patients with ALS. ALS/Riluzole Study Group-II. Neurology 47:S86–S90. CrossRef Medline

Niebrój-Dobosz I, Dziewulska D, Kwieciński H (2004) Oxidative damage to proteins in the spinal cord in amyotrophic lateral sclerosis (ALS). Folia Neuropathol 42:151–156. Medline

Prudencio M, Hart PJ, Borchelt DR, Andersen PM (2009) Variation in aggregation propensities among ALS-associated variants of SOD1: correlation to human disease. Hum Mol Genet 18:3217–3226. CrossRef Medline

Rakhit R, Robertson J, Vande Velde C, Horne P, Ruth DM, Griffin J, Cleveland DW, Cashman NR, Chakrabartty A (2007) An immunological epitope selective for pathological monomer-misfolded SOD1 in ALS. Nat Med 13:754–759. CrossRef Medline

Ralph GS, Radcliffe PA, Day DM, Carthy JM, Leroux MA, Lee DC, Wong LF, Bilsland LG, Greensmith L, Kingsman SM, Mitrophanous KA, Mazarakis ND, Azzouz M (2005) Silencing mutant SOD1 using RNAi protects against neurodegeneration and extends survival in an ALS model. Nat Med 11:429–433. CrossRef Medline

Renton AE, Majounie E, Waite A, Simón-Sánchez J, Rollinson S, Gibbs JR, Schymick JC, Laaksovirta H, van Swieten JC, Myllykangas L, Kalimo H,

Paetau A, Abramzon Y, Remes AM, Kaganovich A, Scholz SW, Duckworth J, Ding J, Harmer DW, Hernandez DG, et al. (2011) A hexanucleotide repeat expansion in C9ORF72 is the cause of chromosome 9p21-linked ALS-FTD. Neuron 72:257–268. CrossRef Medline

Rhoads TW, Lopez NI, Zollinger DR, Morré JT, Arbogast BL, Maier CS, DeNoyer L, Beckman JS (2011) Measuring copper and zinc superoxide dismutase from spinal cord tissue using electrospray mass spectrometry. Anal Biochem 415:52–58. CrossRef Medline

Rhoads TW, Williams JR, Lopez NI, Morré JT, Bradford CS, Beckman JS (2013) Using theoretical protein isotopic distributions to parse small-mass-difference post-translational modifications via mass spectrometry. J Am Soc Mass Spectrom 24:115–124. CrossRef Medline

Roberts BR, Tainer JA, Getzoff ED, Malencik DA, Anderson SR, Bomben VC, Meyers KR, Karplus PA, Beckman JS (2007) Structural characterization of zinc-deficient human superoxide dismutase and implications for ALS. J Mol Biol 373:877–890. CrossRef Medline

Rosen DR, Siddique T, Patterson D, Figlewicz DA, Sapp P, Hentati A, Donaldson D, Goto J, O'Regan JP, Deng HX (1993) Mutations in Cu/Zn superoxide dismutase gene are associated with familial amyotrophic lateral sclerosis. Nature 362:59–62. CrossRef Medline

Rumfeldt JA, Lepock JR, Meiering EM (2009) Unfolding and folding kinetics of amyotrophic lateral sclerosis-associated mutant Cu, Zn superoxide dismutases. J Mol Biol 385:278–298. CrossRef Medline

Sahawneh MA, Ricart KC, Roberts BR, Bomben VC, Basso M, Ye Y, Sahawneh J, Franco MC, Beckman JS, Estévez AG (2010) Cu, Zn-superoxide dismutase increases toxicity of mutant and zinc-deficient superoxide dismutase by enhancing protein stability. J Biol Chem 285: 33885–33897. CrossRef Medline

Son M, Puttaparthi K, Kawamata H, Rajendran B, Boyer PJ, Manfredi G, Elliott JL (2007) Overexpression of CCS in G93A-SOD1 mice leads to accelerated neurological deficits with severe mitochondrial pathology. Proc Natl Acad Sci U S A 104:6072–6077. CrossRef Medline

Soon CP, Donnelly PS, Turner BJ, Hung LW, Crouch PJ, Sherratt NA, Tan JL, Lim NK, Lam L, Bica L, Lim S, Hickey JL, Morizzi J, Powell A, Finkelstein DI, Culvenor JG, Masters CL, Duce J, White AR, Barnham KJ, et al (2011) Diacetylbis(N(4)-methylthiosemicarbazonato) copper(II) (CuII(atsm)) protects against peroxynitrite-induced nitrosative damage and prolongs survival in amyotrophic lateral sclerosis mouse model. J Biol Chem 286:44035–44044. CrossRef Medline

Sreedharan J, Blair IP, Tripathi VB, Hu X, Vance C, Rogelj B, Ackerley S, Durnall JC, Williams KL, Buratti E, Baralle F, de Belleroche J, Mitchell JD, Leigh PN, Al-Chalabi A, Miller CC, Nicholson G, Shaw CE (2008) TDP-43 mutations in familial and sporadic amyotrophic lateral sclerosis. Science 319:1668–1672. CrossRef Medline

Subramaniam JR, Lyons WE, Liu J, Bartnikas TB, Rothstein J, Price DL, Cleveland DW, Gitlin JD, Wong PC (2002) Mutant SOD1 causes motor neuron disease independent of copper chaperone-mediated copper loading. Nat Neurosci 5:301–307. CrossRef Medline

Tiwari A, Liba A, Sohn SH, Seetharaman SV, Bilsel O, Matthews CR, Hart PJ, Valentine JS, Hayward LJ (2009) Metal deficiency increases aberrant hydrophobicity of mutant superoxide dismutases that cause amyotrophic lateral sclerosis. J Biol Chem 284:27746–27758. CrossRef Medline

Tokuda E, Ono S, Ishige K, Watanabe S, Okawa E, Ito Y, Suzuki T (2008) Ammonium tetrathiomolybdate delays onset, prolongs survival, and slows progression of disease in a mouse model for amyotrophic lateral sclerosis. Exp Neurol 213:122–128. CrossRef Medline

Tokuda E, Okawa E, Watanabe S, Ono S, Marklund SL (2013) Dysregulation of intracellular copper homeostasis is common to transgenic mice expressing human mutant superoxide dismutase-1s regardless of their copper-binding abilities. Neurobiol Dis 54:308–319. CrossRef Medline

Urushitani M, Ezzi SA, Julien JP (2007) Therapeutic effects of immunization with mutant superoxide dismutase in mice models of amyotrophic lateral sclerosis. Proc Natl Acad Sci U S A 104:2495–2500. CrossRef Medline

Valentine JS, Pantoliano MW, McDonnell PJ, Burger AR, Lippard SJ (1979) pH-dependent migration of copper(II) to the vacant zinc-binding site of zinc-free bovine erythrocyte superoxide dismutase. Proc Natl Acad Sci U S A 76:4245–4249. CrossRef Medline

Wang J, Slunt H, Gonzales V, Fromholt D, Coonfield M, Copeland NG, Jenkins NA, Borchelt DR (2003) Copper-binding-site-null SOD1 causes ALS in transgenic mice: aggregates of non-native SOD1 delineate a common feature. Hum Mol Genet 12:2753–2764. CrossRef Medline

Wang Q, Johnson JL, Agar NY, Agar JN (2008) Protein aggregation and protein instability govern familial amyotrophic lateral sclerosis patient survival. PLoS Biol 6:e170. CrossRef Medline

Wong PC, Pardo CA, Borchelt DR, Lee MK, Copeland NG, Jenkins NA, Sisodia SS, Cleveland DW, Price DL (1995) An adverse property of a familial ALS-linked SOD1 mutation causes motor neuron disease characterized by vacuolar degeneration of mitochondria. Neuron 14:1105–1116. CrossRef Medline

Zetterström P, Stewart HG, Bergemalm D, Jonsson PA, Graffmo KS, Andersen PM, Brännström T, Oliveberg M, Marklund SL (2007) Soluble misfolded subfractions of mutant superoxide dismutase-1s are enriched in spinal cords throughout life in murine ALS models. Proc Natl Acad Sci U S A 104:14157–14162. CrossRef Medline